Primljen / Received: 4.9.2022.
Ispravljen / Corrected: 4.2.2023.
Prihvaćen / Accepted: 12.3.2023.
Dostupno online / Available online: 10.5.2023.

Effect of soil on the capacity of viscous dampers between adjacent buildings

Authors:

Assoc.Prof. **Elif Cagda Kandemir**, PhD. CE
Izmir Democracy University, Izmir, Turkey
Department of Civil Engineering
elifcagda.kandemir@idu.edu.tr
Corresponding author

Prof. **Robert Jankowski**, PhD. CE
Gdańsk University of Technology, Poland
Faculty of Civil and Environmental Engineering
jankowr@pg.edu.pl

Original research paper

Elif Cagda Kandemir, Robert Jankowski

Effect of soil on the capacity of viscous dampers between adjacent buildings

This study investigated the seismic pounding of two adjacent buildings considering soil–structure interaction (SSI). A comprehensive parametric study of buildings with different heights was performed to reveal the pounding-involved behaviour considering the soil effect. Wavelet transform has been conducted to gain insight into the differences in the frequency contents of the impact forces between fixed- and flexible-base adjacent structures. Linear viscous dampers (LVDs) between adjacent floors were used as pounding protection measures. The required supplemental damping ratio of the LVDs was determined through optimisation analysis under different soil types to verify the effect of the SSI on structural damping. Comparative results with and without SSI showed that incorporating the SSI worsens the pounding-involved responses during earthquakes.

Key words:
adjacent buildings, soil–structure interaction (SSI), continuous wavelet transform, linear viscous damper

Izvorni znanstveni rad

Elif Cagda Kandemir, Robert Jankowski

Učinak tla na kapacitet viskoznih prigušivača između susjednih zgrada

U istraživanju se ispitivao seizmički sudar dviju susjednih zgrada uzimajući u obzir interakciju tla i konstrukcije (engl. *soil-structure interaction* - SSI). Provedena je sveobuhvatna parametarska analiza zgrada različitih visina kako bi se ispitalo ponašanje uzrokovano sudarima, uzimajući u obzir učinak tla. Provedena je valična transformacija (engl. *wavelet transform*) kako bi se dobio uvid u razlike u učestalosti udarnih sila između susjednih konstrukcija s nepomičnom i s fleksibilnom bazom. Linearni viskozni prigušivači (LVD) između susjednih katova upotrijebljeni su kao mjere zaštite od sudara. Potreban dodatni omjer prigušenja LVD-ova određen je optimizacijskom analizom pri različitim vrstama tla kako bi se potvrdio učinak SSI-ja na konstrucijsko prigušenje. Usporedni rezultati s SSI-jem i bez njega pokazali su da uključivanje SSI-ja pogoršava odzive uzrokovane sudarima tijekom potresa.

Ključne riječi:
susjedne zgrade, interakcija tla i konstrukcije (SSI), neprekidno valična transformacija, linearni viskozni prigušivač

1. Introduction

During severe earthquakes, adjacent structures are prone to major damage or even collapse owing to their asynchronous oscillations, as experienced in many recent earthquakes, such as the 2011 Christchurch Earthquake [1], 2011 Van Earthquake [2], and 2015 Gorkha Earthquake [3]. For more than three decades, researchers have investigated seismic pounding and they have published the results of the studies in several papers [4-12]. The different structural configurations, impact models, analyses, and assumptions considered in these studies have indicated that structural pounding amplifies structural responses. Another exaggerating factor is the soil effect, which involves the sliding, rotation, and settlement of foundations during earthquakes [13-21]. The assumption of a fixed base that neglects the soil effect is sufficient for structures with low structural rigidity, in which the displacement of the superstructure is more important than that of the foundation. Nevertheless, the soil effect must be considered because in more rigid structures, foundation moments may contribute excessively to the overall response and stiffness [22]. Mahmoud et al. [23] analysed adjacent 3-storey buildings with a flexible base. According to the results, in terms of the weight and stiffness of neighbouring structures, the response of lighter structures increased when the soil effect was considered. Ghandil and Aldaikh [24] investigated the separation distance and damage distribution along building heights of flexible-base adjacent structures. They stated that the separation distance must be three times the minimum distance stipulated in the 1997 International Building Code. Madani et al. [25] also demonstrated ascending pounding forces between two adjacent buildings under flexible-base conditions with varying separation gaps and structural heights. Naserkhaki et al. [26] investigated both pounding and soil–structure interaction (SSI) effect on multi-storey buildings during ground motions modelled using sine waves and applied actual earthquake records. They remarked that the increase in seismic responses was too large to ignore the soil effects.

Both pounding and soil effects can cause destructive damage to structures and should be controlled and mitigated. The efficiency of viscous dampers to suppress the aggravated structural vibration of adjacent structures due to SSI have been studied by Kazemi et al. [10], Elwardany et al. [12], Kermani et al. [27], and Miari and Jankowski [28]. Sarcheshmehpour et al. [29] implemented viscous dampers in flexible-base steel frames using genetic algorithm optimisation. They concluded that damping decreased when the soil effect was considered. Kazemi et al. [11] used linear and nonlinear viscous dampers between adjacent moment-resisting structures considering the soil effect. They showed that the probability of collapse during pounding decreases after the viscous damper linkage.

This study investigated the pounding behaviour of two adjacent buildings and the required viscous damper capacity to prevent impact by considering the SSI. In a previous study [30], fixed-base adjacent structures and their links using linear viscous dampers (LVDs) were investigated. For comparison, analyses were performed using the same structural models. Three cases associated with two buildings with different masses, stiffness parameters, and heights were investigated. In case 1, the mass and stiffness parameters of each floor of both structures were the same, whereas they varied in cases 2 and 3. The number of floors in one of the buildings was changed from one to 15, whereas the other was a 15-storey building. The buildings were assumed to be shear-beam-type structures and were modelled as lumped mass–stiffness systems with one translational degree of freedom per mass and linear force–deformation characteristics. Although most structures exhibit nonlinear behaviour under seismic loads, the assumption of linear elastic behaviour is adequate for structures with seismic energy dissipation devices, particularly in the preliminary design step [31-35]. The Rayleigh damping matrices were constructed at a damping ratio of 5 %. Earthquake-induced pounding was assumed to occur only between adjacent floor levels and floor elevations of 3.6 m in all buildings. The impact between the floors was modelled using a linear spring and dashpot in parallel, i.e. the Kelvin–Voigt model. Pounding forces of fixed and flexible-base structures were also evaluated using continuous wavelet transform (CWT) to derive the frequency components of a collision on a time scale. LVDs were used as pounding-protection measures between adjacent storeys. The supplemental damping ratios and LVD capacities were optimised to determine the minimum total damper capacity which prevents pounding between adjacent floors. The damper capacities were compared with those obtained for fixed-base buildings. This paper aims to contribute to the recent literature by considering the results of additional damping ratios required when SSI is considered. All analyses and the model setup were conducted using MATLAB software [36].

2. Numerical models

2.1. Impact model

Impact models, such as the linear viscoelastic model by Anagnostopoulos [37], nonlinear elastic model by Davis [38], and nonlinear viscoelastic model by Jankowski [39], have been developed and used in many structural systems [40-43]. In this study, the linear viscoelastic model, also known as the Kelvin–Voigt model, was used. The model parameters, consisting of a linear spring and dashpot in parallel, are expressed as follow [37]:

$$F_p(t) = k_p\delta(t) + c_p\dot{\delta}(t) \tag{1}$$

$$c_p = 2\xi_p\sqrt{k_p\frac{m_1 m_2}{m_1+m_2}} \tag{2}$$

$$\xi_p = \frac{-\ln e}{\sqrt{\pi^2+(\ln e)^2}} \tag{3}$$

where $F_p(t)$ is the pounding force as a function of time (t), k_p is stiffness, and c_p is the damping coefficient of the impact model. $\delta(t)$ and $\dot{\delta}$ are the relative displacement and relative velocity between two colliding structural members, respectively. ξ_p is the impact damping ratio, and e is the coefficient of restitution. The masses of the colliding members are denoted by m_1 and m_2. In this study, k_p was set to be 20 times the storey stiffness coefficient of the stiffer structure, as considered by Anagnostopoulos [37]. Moreover, ξ_p qual to 0.14 (e = 0.65), was used for concrete surfaces, as suggested by Azevedo and Bento [44]. A linear spring and dashpot were activated when the gap between the structures was closed, thereby generating a pounding force.

2.2. Soil–structure interaction mechanism

The sway-rocking model, which idealises the soil beneath a structure using springs and dashpots for translational and rotational movements, was used in this study. The soil is considered a homogeneous, linearly elastic, and isotropic half-space, described by its shear modulus G, Poisson"s ratio ν, mass density ν, and shear wave velocity V_s. For the structures considered herein, a 17 m ×17 m mat foundation was assumed, as discussed by Sarcheshmehpour et al. [29] for three-, seven- and 14- storey buildings. According to Wolf"s equation [45], the equivalent radius (r) of the foundation was obtained using $\sqrt{A/\pi}$ as 10 m, where A is the area of the foundation. The Turkish Building Earthquake Code 2018 (TBEC 2018) [46] classifies soil into six types, from hard soil (ZA) to soil with special treatment requirements (ZF), which is similar to ASCE 7-16 [47]. Five of them, ZA (hard rock), ZB (rock), ZC (very dense soil and soft rock), ZD (stiff soil), and ZE (loose sand) were considered in this research. The soil characteristics are presented in Table 1.

Table 1. Soil types and their properties

Soil types	Poisson"s ratio (ν)	Mass density (ρ) [kNs/m⁴]
ZA (hard rock)	0.20 [39]	2.40 [41]
ZB (rock)	0.25 [39]	2.25 [41]
ZC (soft rock)	0.33 [40]	2.00 [41]
ZD (stiff soil)	0.40 [40]	1.80
ZE (loose sand)	0.50 [40]	1.50

The equations for the stiffness and damping coefficients of the soil provided in the study by Veletsos and Ventura [51] are expressed as follows:

$$K_h = 8Gr/(2\text{-}\nu) \quad (4a)$$

$$C_h = 4{,}6\rho V_s r^2/(2\text{-}\nu) \quad (4b)$$

$$K_\theta = 8Gr^3/(3\text{-}3\nu) \quad (5a)$$

$$C_\theta = 0{,}46\rho V_s r^4/(1\text{-}\nu) \quad (5b)$$

where K_h and K_θ are static translational and rotational stiffness coefficients, and C_h and C_θ are damping coefficients along the sliding and rocking directions, respectively. The soil shear modulus is calculated using $G = \rho V_s^2$.

2.3. Equation of motion and optimization procedure

Two adjacent multi-storey buildings, which were assumed to be shear-beam systems, were modelled using lumped mass–stiffness models. The height of each storey was the same at 3.6 m. A uniform distribution of stiffness and mass was adopted. The mass of each storey (1×10^5 kg) was lumped at the slab level. The storey stiffness of building 1 was 6.8×10^7 N/m, whereas those of the other buildings were 6.8×10^7 N/m (case 1), 10×10^8 N/m (case 2), and 7.2×10^6 N/m (case 3). The structural properties and cases considered are listed in Table 2. Hereafter, building 2 in cases 2 and 3 is referred to as a stiffer and more flexible structure, respectively. The number of storeys of building 2 was varied from 1 to 15 to simulate construction steps and/or neighbouring buildings of different heights. The seismic gap between buildings was computed based on the building height, as regulated in TBEC 2018 [46], which states that for buildings with a total height of up to 6 m, the separation distance is 30 mm, and an additional 10 mm is added for every subsequent 3 m of height. The configurations of the multi-storey buildings are shown in Figure 1. For adjacent buildings with *l* and *r* storeys connected by LVDs, the coupled equation of motion is expressed as

$$M\ddot{X} + \left(C^{(s)} + Cd\right)\dot{X} + KX + F_p = -Mr\ddot{x}_g \quad (6)$$

where the size of each matrix (***M***, ***K***, ***C***), including soil features, is *l*+*r*+4 (the sum of lumped mass translations and four degrees of freedom for rocking and swaying of the foundation). The superscript

Table 2. Building properties and considered cases

Cases	m [kg]	Building 1			Building 2		
		k [N/m]	Storey number	Storey height [m]	k [N/m]	Storey number	Storey height [m]
Case 1	$1 \cdot 10^5$	$6.8 \cdot 10^7$	15	3.6	$6.8 \cdot 10^7$	1-15	3.6
Case 2					$10 \cdot 10^8$		
Case 3					$7.2 \cdot 10^6$		

s in Equation (6) denotes the building number (1 for building 1 and 2 for building 2). In Figure 1, each structural parameter *m*, *k* and *c* has subscripts indicating the storey number and building number after the comma. The number of attached viscous dampers was equal to the number of storeys of the shorter building.

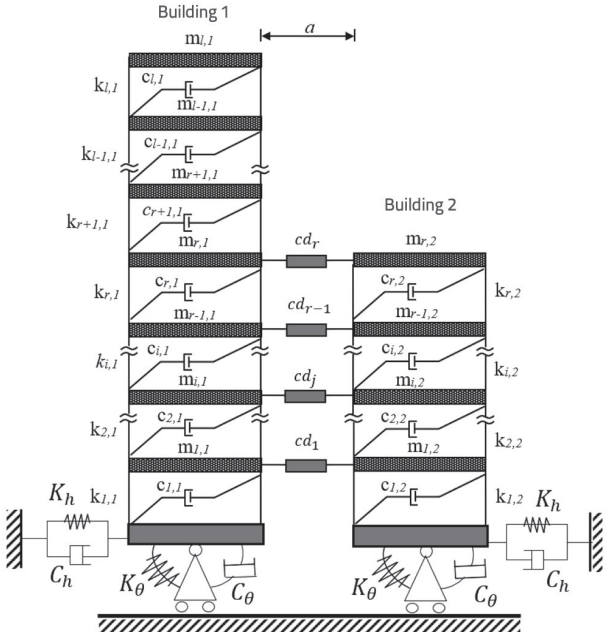

Figure 1. Configuration of adjacent buildings

The matrices are expressed as

$$\underset{(l+r+4,l+r+4)}{\boldsymbol{M}} = \begin{bmatrix} [\boldsymbol{M}^{(1)}]_{(l,l)} & [\boldsymbol{m}_i^{(1)}]_{(l,1)} & [\boldsymbol{m}_i^{(1)}\boldsymbol{h}_i^{(1)}]_{(l,1)} & 0 & \cdots & 0 \\ [\boldsymbol{m}_i^{(1)}]_{(1,l)} & \Sigma \boldsymbol{m}_i^{(1)} & \Sigma(\boldsymbol{m}_i^{(1)}\boldsymbol{h}_i^{(1)}) & \vdots & \ddots & \vdots \\ [\boldsymbol{m}_i^{(1)}\boldsymbol{h}_i^{(1)}]_{(1,l)} & \Sigma(\boldsymbol{m}_i^{(1)}\boldsymbol{h}_i^{(1)}) & \Sigma \boldsymbol{m}_i^{(1)}(\boldsymbol{h}_i^{(1)})^2 & 0 & \cdots & 0 \\ 0 & \cdots & 0 & [\boldsymbol{M}^{(2)}]_{(r,r)} & [\boldsymbol{m}_i^{(2)}]_{(r,1)} & [\boldsymbol{m}_i^{(2)}\boldsymbol{h}_i^{(2)}]_{(r,1)} \\ \vdots & \ddots & \vdots & [\boldsymbol{m}_i^{(2)}]_{(1,r)} & \Sigma \boldsymbol{m}_i^{(2)} & \Sigma(\boldsymbol{m}_i^{(2)}\boldsymbol{h}_i^{(2)}) \\ 0 & \cdots & 0 & [\boldsymbol{m}_i^{(2)}\boldsymbol{h}_i^{(2)}]_{(1,r)} & \Sigma(\boldsymbol{m}_i^{(2)}\boldsymbol{h}_i^{(2)}) & \Sigma(\boldsymbol{m}_i^{(2)}\boldsymbol{h}_i^{(2)}) \end{bmatrix} \tag{7a}$$

$$\underset{(l+r+4,l+r+4)}{\boldsymbol{K}} = \begin{bmatrix} [\boldsymbol{K}^{(1)}]_{(l,l)} & 0 & \cdots & & 0 \\ 0 & K_h^{(1)} & & & \\ & & K_\theta^{(1)} & \ddots & \vdots \\ \vdots & & \ddots & [\boldsymbol{K}^{(2)}]_{(r,r)} & \\ & & & & K_h^{(2)} \; 0 \\ 0 & \cdots & & 0 & 0 \; K_\theta^{(2)} \end{bmatrix} \tag{7b}$$

$$\underset{(l+r+4,l+r+4)}{\boldsymbol{C}} = \begin{bmatrix} [\boldsymbol{C}^{(1)}]_{(l,l)} & 0 & \cdots & & 0 \\ 0 & C_h^{(1)} & & & \\ & & C_\theta^{(1)} & \ddots & \vdots \\ \vdots & & \ddots & [\boldsymbol{C}^{(2)}]_{(r,r)} & \\ & & & & C_h^{(2)} \; 0 \\ 0 & \cdots & & 0 & 0 \; C_\theta^{(2)} \end{bmatrix} \tag{7c}$$

$$\underset{(l+r+4,l+r+4)}{\boldsymbol{Cd}} = \begin{bmatrix} [\boldsymbol{A}]_{(r,r)} & [0]_{(r,l-r+2)} & [-\boldsymbol{A}]_{(r,r)} & [0]_{(r,2)} \\ [0]_{(l-r+2,r)} & [0]_{(l-r+2,l-r+2)} & [0]_{(l-r+2,r)} & [0]_{(m-r+2,2)} \\ [-\boldsymbol{A}]_{(r,r)} & [0]_{(r,l-r+2)} & [\boldsymbol{A}]_{(r,r)} & [0]_{(r,2)} \\ [0]_{(2,r)} & [0]_{(2,l-r+2)} & [0]_{(2,r)} & [0]_{(2,2)} \end{bmatrix} \tag{7d}$$

where the mass matrices of the buildings are $[M^{(1)}] = \text{diag}(m_{i,1})$ and $[M^{(2)}] = \text{diag}(m_{i,2})$. The subscript *i* is the storey number of the corresponding building 1 or 2. *h* is the storey height calculated from the base. Matrix dimensions are given in parentheses. *Cd* is the damping coefficient matrix of LVDs attached between adjacent floors. In *Cd*, $[A] = \text{diag}(cd)$ i $[-A] = \text{diag}(-cd)$.

The number of dampers is equal to the number of storeys in building 2 (storeys changing from 1 to 15); therefore, the damper coefficient vector has *r* rows, $\text{cd} = \{cd_1, \ldots, cd_j, \ldots, cd_r\}$.

The supplemental damping ratio for adjacent structures of flexible-base adjacent structures is given as [30]:

$$\xi_d^s = \frac{\left(\max\left\{T_{1,1}^f, T_{1,2}^f\right\}\right)\sum_j cd_j\left(\phi_{1,1}^f - \phi_{1,2}^f\right)^2}{4\pi\sum_i m_i\phi_i^{f2}} \tag{8}$$

where the superscript *f* denotes the parameters of flexible-base structures, $T_{1,1}^f, T_{1,2}^f$ are the natural periods, and $\phi_{1,1}^f$, $\phi_{1,2}^f$ are the mode shapes of buildings 1 and 2, respectively, calculated through eigenvalue analysis. In the optimisation procedure addressed herein, the objective function is the minimisation of the total damper capacity with a uniform distribution among adjacent floors. This study aimed to prevent pounding by adjusting the supplemental damping ratio. The minimum total damper capacity was obtained through a constrained optimisation study performed using the *fmincon* function in MATLAB [30, 36]. This function requires the lower and upper constraints assigned as zero to represent the no-damper case and an arbitrary value for the predefined maximum damper capacity, respectively. The equality constraint ($A_{eq(j)}$) based on Equation (8) is derived as follows:

$$\left\{A_{eq(j)}\right\} = \frac{\left(\max\left\{T_{1,1}^f, T_{1,2}^f\right\}\right)}{4\pi\sum_{i=1}^{l+r} m_i\phi_i^{f2}}\left(\phi_{1,1}^f - \phi_{1,2}^f\right)^2 \tag{9}$$

$$\left\{A_{eq}^s\right\} = \left\{A_{eq(1)}^f, \ldots, A_{eq(j)}^f, \ldots, A_{eq(r)}^f\right\} \tag{10}$$

$$\left\{A_{eq}^s\right\}\left[cd\right] = \xi_d^f \tag{11}$$

The product of the equality constraint and the damper coefficient vector provides the supplemental damping ratio ξ_d^f. This ratio is gradually increased, and the damper coefficient vector *cd* is searched until the pounding forces at all floors are zero.

Table 3. Selected ground motions

Earthquake	Station	PGA [g]	PGV [m/s]	PGA/PGV	Magnitude (M_w)
Duzce, 1999	Bolu	0.739	0.583	1.268	7.2
Kobe, 1995	JMA	0.834	0.902	0.925	6.9
Samos, 2020	Kusadasi	0.183	0.225	0.813	6.6

3. Ground motions

In this paper, examples of the results achieved for selected ground motions with different magnitudes, peak ground accelerations (PGAs), and peak ground velocities (PGVs) are introduced (see Table 4). Note that the Duzce and Kobe earthquakes are examples of strong near-fault earthquakes, and the Samos earthquake is the latest strong earthquake which occurred in Turkey. The acceleration records of the 1995 Kobe and 1999 Duzce earthquakes were derived from the PEER ground motion database [52], and the 2020 Samos earthquake acceleration record was obtained from the AFAD database [53].

4. Results

The comparative results of the fixed- and flexible-base structures are presented in this section to clarify the effect of SSI on the pounding-involved seismic responses.

4.1. Pounding forces and evaluation using wavelet transform

The pounding forces is depicted based on the nondimensional frequency parameter ratio between adjacent structures. This parameter is defined as the normalised quantity for various storey numbers [30]. For each building, it was calculated using $\Omega_i = \omega_i s_i^2 \sqrt{m_i / k_i}$, where i (i = 1, 2) is the building number, ω_i and s_i are the natural angular frequency and storey number, respectively, whereas m_i and k_i are the mass and stiffness parameters of one storey of the corresponding building, respectively. The ratio representing the normalised value between adjacent buildings was computed using $\Omega_r = \Omega_2 / \Omega_1$.This ratio provides a nondimensional scale for comparison of the results presented in this section instead of using the frequency ratio, which depends on the structural properties.

The cumulative impact forces based on the nondimensional frequency parameter ratio are presented in Figures 2 to 4 for fixed- and flexible-base structures founded on ZC-type soil and exposed to the Duzce, Kobe, and Samos earthquakes. The impact forces obtained in case 3 (indicated in yellow) appeared to be larger in each graph, regardless of whether the structure had a fixed or flexible base. Thus, we can conclude that a more flexible neighbouring building (case 3) worsens the pounding responses as the number of storeys increases. The trends in the cumulative pounding forces of both the fixed- and flexible-base structures during the Duzce earthquake (Figure 2) were similar, revealing that greater forces were obtained as the heights of the structures approached each other. In case 1, the largest pounding force of approximately 2×10^8 N occurred for the 11-storey building; however, an impact force of 45×10^8 N was obtained for the 3-storey building with SSI. Nevertheless, for case 2, the largest pounding force was approximately 2×10^8 N for the structure with a fixed base and 10×10^8 N for the structure with SSI when both pounded a 14-storey building. The importance of considering the SSI during the building analysis

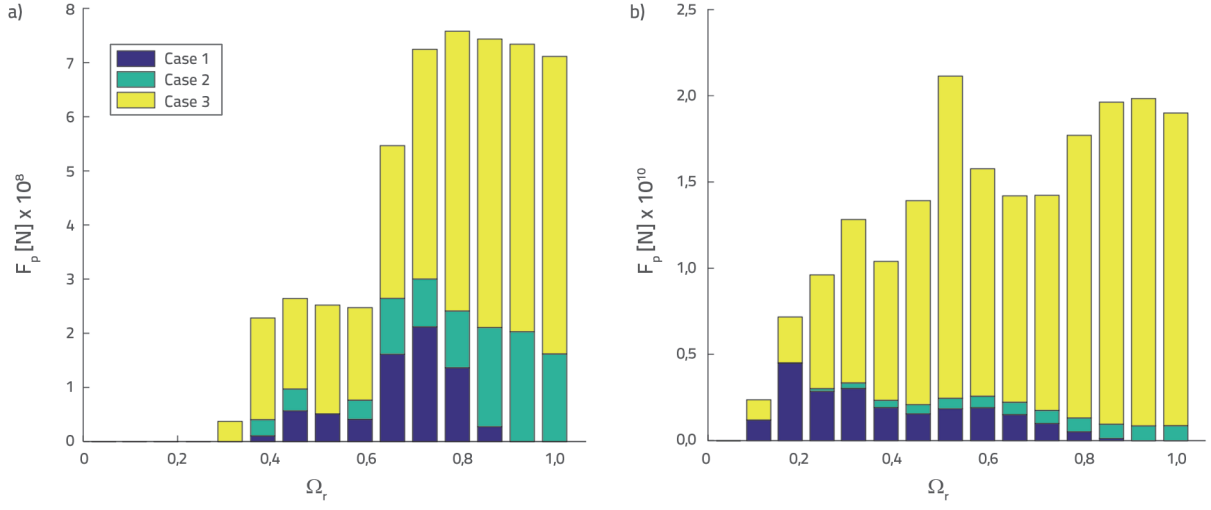

Figure 2. Impact forces based on nondimensional frequency parameter ratio, Ω_r: a) fixed-base; b) flexible-base structures founded on ZC-type soil under the Duzce earthquak

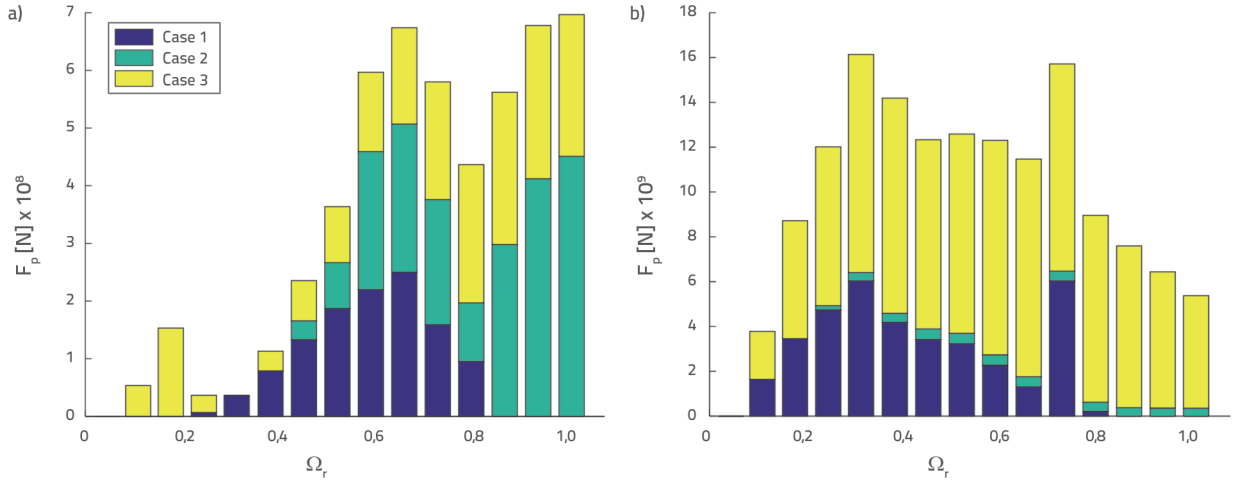

Figure 3. Impact forces based on nondimensional frequency parameter ratio, Ω_r: a) fixed-base; b) flexible-base structures founded on ZC-type soil under the Kobe earthquake

became clear for case 3, in which the pounding forces were 5.5×10^8 N for the fixed base and 200×10^8 N for the SSI in the 15-storey building. Regarding the Kobe earthquake (Figure 3), the cumulative pounding behaviour was very similar to that of the Duzce earthquake.

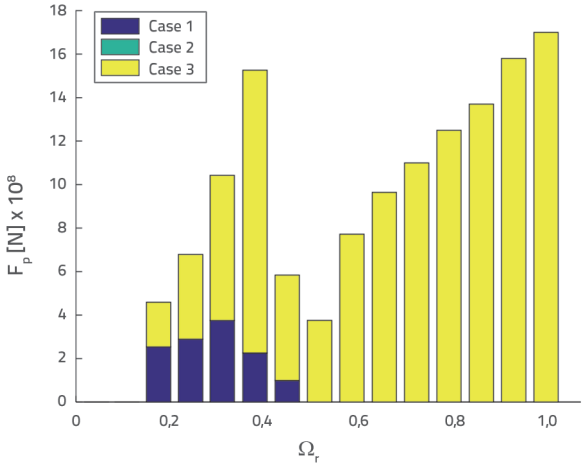

Figure 4. Impact forces based on nondimensional frequency parameter ratio, Ω_r: flexible-base structures founded on ZC-type soil under the Samos earthquake

In case 1, a pounding force of 2.5×10^8 N was computed for a 10-storey building, whereas 60×10^8 N occurred for 5- and 11-storey buildings with SSI. Pounding forces were almost same in case 2, 4.5×10^8 N for a 15-storey building with a fixed base, and 4×10^8 N for a 10-storey building with SSI. In case 3, a pounding force of 2.25×10^8 N was obtained for a 12-storey building and 100×10^8 N was obtained for a 10-storey building with SSI. Therefore, these numerical results show that the SSI should be considered in the event of a collision with a more flexible building. The relatively lower PGA of the Samos earthquake resulted in no collision between fixed-base buildings; in contrast, for flexible-base buildings, large pounding forces were observed for cases 1 and 3, except for case 2, as presented in Figure 4. From these figures, we can deduce that the pounding force is highly dependent on the flexibility of neighbouring structures. Being adjacent to the low-stiffness structure caused a greater pounding force of approximately 17×10^8 N, as in case 3. In addition, the SSI had an increasing effect on the pounding responses, regardless of the rigidity of the neighbouring structures and earthquake characteristics.

The pounding force responses of case 3, under the Duzce and Kobe earthquakes, were also processed using a CWT. However, note that the wavelet scalograms could not be presented for the Samos earthquake because no pounding occurred for the fixed-base case, thus offering no possibility to compare the responses. Wavelet transform is a suitable tool for nonstationary signals because it decomposes the signal into basic functions of dilated (scaled) and translated (shifted) versions of the mother wavelet function, simultaneously supplying frequency–time knowledge of the signal. Unlike Fourier transform, wavelet analysis can present the frequency components of any signal in the time domain [54, 55]. There are two types of wavelet transforms: discrete and continuous. The scale and shifting parameters during windowing make them different. The discrete wavelet transform uses only a subset of scale and shifting parameters, whereas the CWT computes the wavelet coefficients at each scale in discrete time. Despite the heavy computer load, the latter was used in this study owing to its windowing capability to provide frequency information. The wavelet coefficients $C(a,b)$, as functions of a and b, were obtained by multiplying the original signal by appropriately scaled and shifted wavelets, as follows [56]:

$$C(a,b)=\int_{-\infty}^{\infty} f(t)\cdot\psi(a,b,t)\,dt \tag{12a}$$

$$\psi(a,b,t)=\frac{1}{\sqrt{a}}\psi^{*}\left(\frac{t-b}{a}\right) \tag{12b}$$

where $\psi(a, b, t)$ is the main wavelet, and a a, b, t are the time, scale, and shifting factors, respectively. ψ^* is a complex conjugate of wavelets. Consequently, the correlation coefficient of the scaled wavelet with the signal was plotted on a scale–time graph. The scalogram of the CWTs revealed the correlation between the scaled (a) and shifted (b) wavelets and the signal in the scale–time plane. According to the default colouring, blue indicates a low correlation and red denotes a high correlation. The scale parameter (a) is the inverse of frequency with respect to multiplication. Thus, low-scale values indicate high-frequency content in the signal, and high-scale values denote low-frequency content. Additionally, abrupt variations in the signal

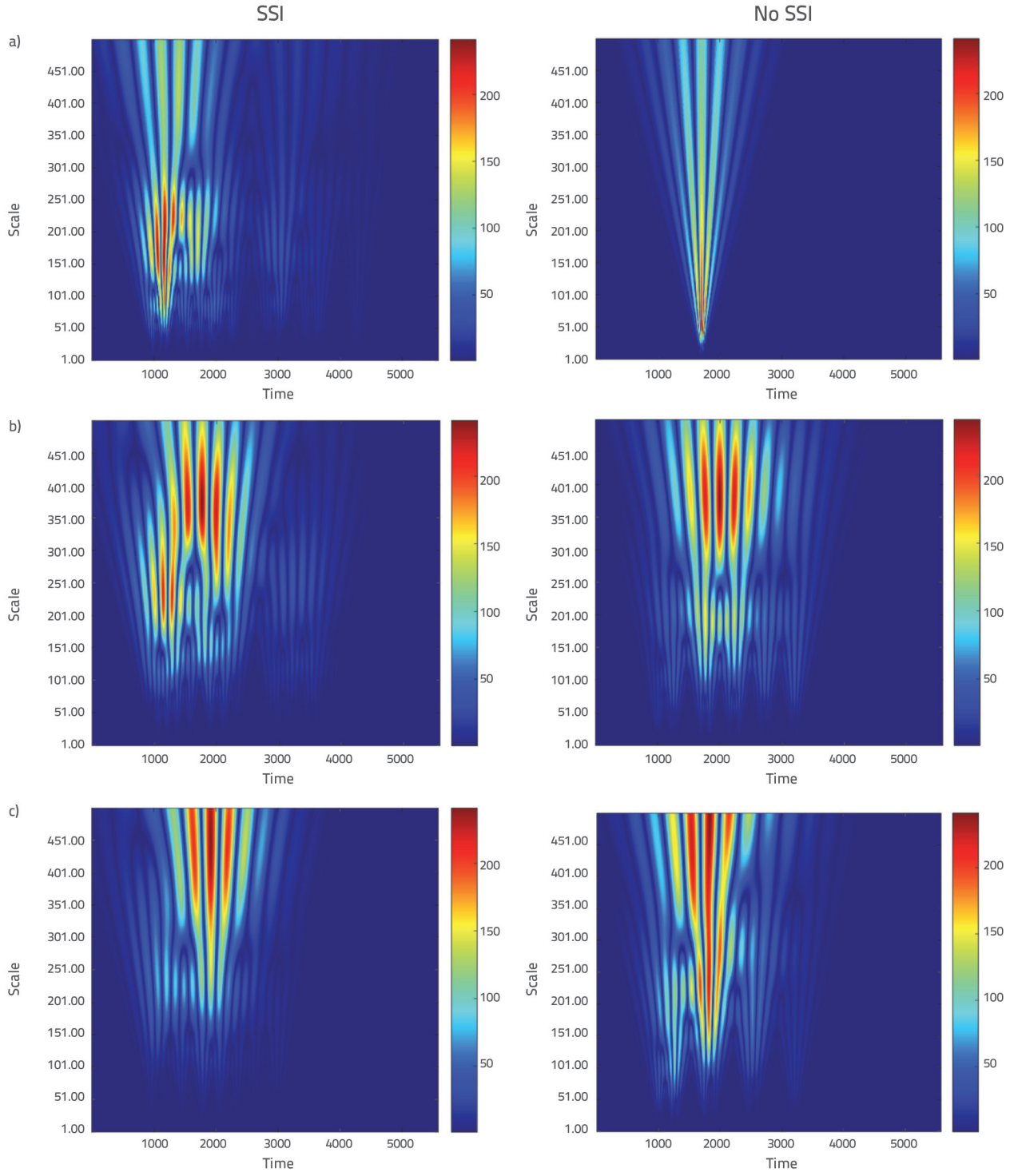

Figure 5. Wavelet scalogram of impact forces in case 3 under the Duzce earthquake: a) 15/5 storeys; b) 15/10 storeys; c) 5/15 storeys

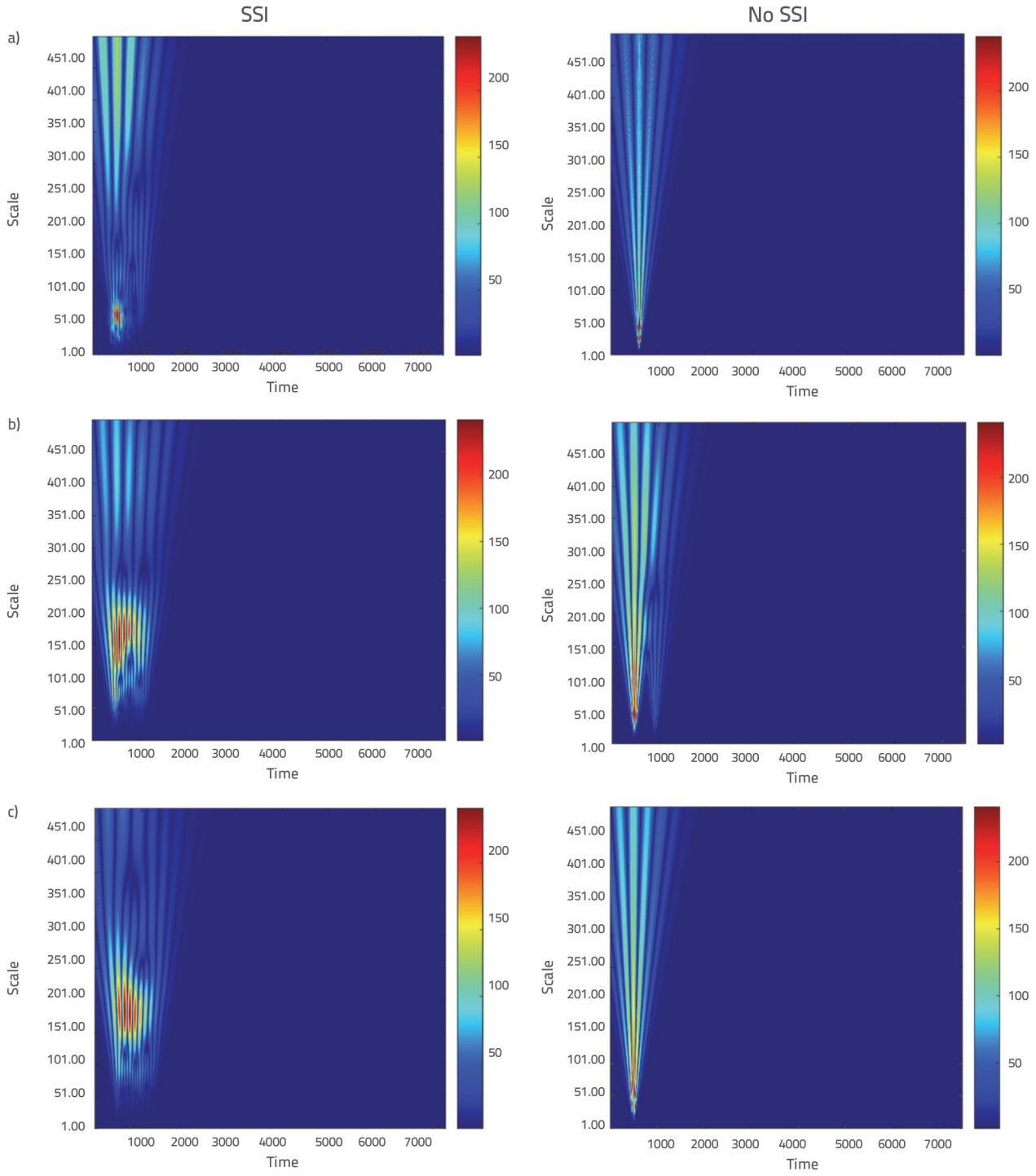

Figure 6. Wavelet scalogram of impact forces in case 3 under the Kobe earthquake: a) 15/5 storeys; b) 15/10 storeys; c) 15/15 storeys

can be detected using low-scale wavelets, whereas slower variations can be detected with high-scale wavelets. Various wavelets are available, such as Haar, Morlet, Daubechies, and Mexican Hat. The Morlet wavelet, which was used in this study, is a complex function that has proven to be an effective tool for feature extraction in mechanical vibration signal diagnosis [57, 58]. It has also been applied to seismic-signal detection [59, 60]. CWT analysis was conducted using MATLAB [36] (see the results in Figures 5 and 6). The pounding forces were calculated using the Kelvin–Voigt model in the time domain and were transformed into constituent wavelets. In the time-domain analysis, we can observe the signal with its value at a specific time; however, in the frequency-domain analysis using CWT, we can derive the frequency content of the signal at a specified time. In the wavelet scalograms, the horizontal axis indicates time, whereas the vertical axis denotes the scales, which are

set as 1:1:500. Large-scale coefficients, or the magnitudes of the impact forces, are represented by red waves, whereas relatively lower values are represented by blue waves. The sampling period for CWT is 0.01 s; therefore, we should multiply the time given in the time axis by 100. All figures in this section show a comparison of the wavelet scalograms of the flexible-base structures with those of the fixed-base structures. Figure 5.a shows that during the Duzce earthquake, when the SSI was considered, the maximum pounding force occurred earlier, at approximately 11 s, than in the structure with a fixed base, which had an impact at 18 s. In addition, the red waves extended in higher scales at approximately 200 (frequency equals 1/200), i.e. lower frequencies, which were larger than that of the fixed base (scale was 25), addressed more and severe impact forces. Nevertheless, Figure 5.b and 5.c shows extending blue bulbs for the fixed-base cases, which indicated a large number of pounding incidents. In contrast, as the height of the buildings approached, the maximum impact forces occurred at high scales, i.e. at lower frequencies (1/400), as shown by the red waves, indicating that collisions were detected over longer periods. Regarding the severity of collisions (red waves), the pounding responses were augmented for higher-neighbouring buildings. For the building height, the wavelet scalograms of the pounding forces showed that the number and severity of impacts increased and extended over long periods, such as from 10 to 20 s. Considering SSI, impacts occurred earlier for lower structures of approximately 10 s.

Compared with fixed-base structures, more frequent impacts on flexible-base structures during the Kobe earthquake can be observed in Figure 6, as the waves spread over a wider area. All the collisions occurred during the first 10 s. Although the maximum collisions appeared almost simultaneously, they differed on the scale axis. When the maximum impact occurred, higher scales corresponding to the low-frequency components were observed for the structure subjected to the Kobe earthquake when considering the SSI, particularly when the building height was increased.

4.2. Optimum LVD capacities

LVDs have been used between adjacent floors to prevent earthquake-induced structural pounding. The addition of dampers to the coupled system synchronises the structural behaviour and, consequently, mitigates the seismic responses through the supplemental damping ratio. Therefore, an optimisation study was performed to determine the required damping ratio to prevent pounding between the structures. The optimisation procedure presented here is applicable to all adjacent structures regardless of the model or structural system. This method is based on the structural behaviour during an earthquake rather than on the dynamic characteristics of the structure. The optimisation procedure can be summarised as follows. The supplemental damping ratio is increased gradually at each time step until no pounding occurs. In the optimisation process, if the pounding forces on all the floors are zero, the algorithm is terminated. Otherwise, the upper bound is increased until the no-pounding case is reached at all adjacent storeys. In this study, the upper bound, *ub*, was set as 5×10^5 Ns/m, which was achieved by processing all optimisation cases and finding a value that provided no pounding for each case study.

In this section, the total damping coefficients and damping ratios supplied by the viscous dampers are compared for the fixed- and flexible-base structures. The results were obtained for the ZC-type soil for the flexible-base case and the Duzce earthquake for comparison with the fixed-base results described in the study by Kandemir-Mazanoglu and Mazanoglu [30]. Table 4 presents the optimum supplemental damping ratios and total damper coefficients for the different storeys of building 2 (B2), which was adjacent to the 15-storey building 1 (B1). The 5-, 7-, 9-, 10-, 11-, 13- and 14-storey buildings with flexible bases in case 1; 5-, 7-, 9-, 10-, 11- and 13-storey buildings with flexible bases in case 2; and 2-, 7-, 10-, 11- and 13-storey buildings with flexible bases in case 3 had lower supplemental damping ratios than structures with fixed bases. For case 1, the maximum damping ratio was 65 % for the 7-storey fixed-base structure, whereas 30 % was adequate for the flexible-base structure. However, the corresponding total damper coefficient increased from 1.43 to 25.21×10^5 Ns/m. However, the 14-storey structure with a fixed base required 1579.10×10^5 Ns/m, whereas no damper was required when SSI was considered. In case 2, for the 13-storey building, the damping ratio decreased from 95 % to 20 % for the structure with SSI. The increase in the damping coefficient was 18.73 to 22.58×10^5 Ns/m, which was relatively smaller than that in case 1. However, the 14-storey structure with a fixed base required 1579.10×10^5 Ns/m, whereas a smaller damper capacity of 18.87×10^5 Ns/m was required when SSI was considered. In case 3, higher damping ratios were encountered, as expected, owing to the large impact forces. The maximum reduction in damping ratios was obtained for the 13-storey building, which was reduced from 75 % to 45 %, whereas the increment in damping force was 15.68 to 50.83×10^5 Ns/m. However, the 14-storey structure with fixed base required 1579.10×10^5 Ns/m, whereas a smaller damper capacity with 56.61×10^5 Ns/m was required when SSI was considered. Similar with the results obtained in the previous section regarding the impact forces, the SSI is an important factor to consider for structures subjected to seismic excitation. In this section, the advantage of the LVD capacity in considering the SSI is clarified, particularly for the impact mitigation of tall buildings. In addition, as presented in Figure 7, the additional damping ratio tended to decrease as the heights of both buildings approached each other when considering the SSI in cases 1 and 2; however, when a building was adjacent to a more flexible building, as in case 3, increased the ratio. The results confirmed that the structural modal damping ratio of the fundamental natural period increases with the incorporation of SSI [41], which results in a lower damping ratio that must be supplied by the viscous dampers. The changes in the damper parameters based on the soil type are listed in Table 5. In all

Table 4. Comparison of ξ_d and Σcd in cases 1, 2, and 3

Storey number B1/B2	Ω_r	Case 1		Case 2		Case 3	
		ξ_d [%] (Fixed-base [30])	Σcd (×10⁵ Ns/m) (Fixed-base [30])	ξ_d [%] (Fixed-base [30])	Σcd (×10⁵ Ns/m) (Fixed-base [30])	ξ_d [%] (Fixed-base [30])	Σcd (×10⁵ Ns/m) (Fixed-base [30])
15/01	0.002	-	-	-	-	-	-
15/02	0.015	5 (-)	8.12 (-)	-	-	5 (15)	12.18 (2.62)
15/03	0.036	10 (10)	13.27 (2.70)	5 (-)	6.61 (-)	10 (10)	13.22 (2.67)
15/04	0.067	10 (5)	10.70 (1.99)	10 (-)	10.71 (-)	20 (10)	21.47 (3.99)
15/05	0.107	20 (30)	18.75 (5.41)	15 (35)	14.01 (6.52)	35 (15)	32.84 (2.44)
15/06	0.156	30 (15)	26.00 (13.99)	20 (15)	17.44 (13.99)	30 (10)	26.05 (6.87)
15/07	0.214	30 (65)	25.21 (1.43)	25 (75)	20.96 (17.81)	45 (65)	37.74 (8.75)
15/08	0.281	30 (10)	25.14 (21.45)	30 (10)	25.06 (21.45)	60 (15)	50.11 (18.51)
15/09	0.357	25 (55)	21.32 (11.35)	30 (55)	25.60 (11.35)	65 (65)	55.45 (13.82)
15/10	0.442	20 (55)	17.88 (11.25)	25 (65)	22.27 (13.63)	60 (75)	53.40 (16.19)
15/11	0.536	15 (55)	14.29 (11.18)	25 (95)	23.71 (21.48)	60 (85)	47.42 (18.57)
15/12	0.638	10 (5)	10.30 (138.92)	20 (5)	20.54 (138.92)	50 (5)	51.36 (138.92)
15/13	0.750	5 (20)	2.45 (3.94)	20 (95)	22.58 (18.73)	45 (75)	50.83 (15.68)
15/14	0.871	- (5)	- (1579.10)	15 (5)	18.87 (1579.10)	45 (5)	56.61 (1579.10)
15/15	1	-	-	15 (5)	19.92 (45.00)	25 (5)	25.45 (45.00)

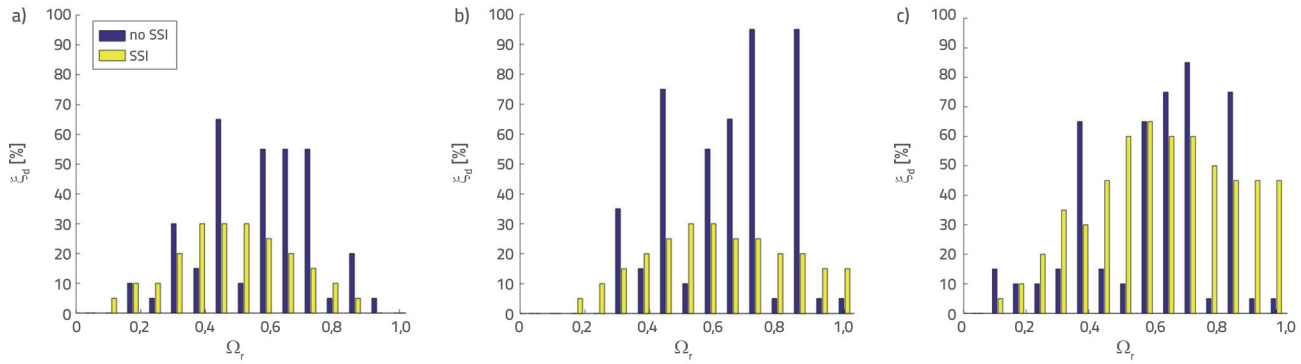

Figure 7. Additional damping ratio based on nondimensional natural period ratio: a) case 1; b) case 2; c) case 3

cases studied, the greatest damping coefficients were obtained for the ZC-type soil at 20 %, 25 %, and 60 %, with corresponding damping coefficients of 17.88×10⁵, 22.27×10⁵, and 53.40×10⁵ Ns/m for cases 1, 2, and 3, respectively, for the 10-storey building. For more flexible soil, the required damping coefficient decreased, such as 9.37×10⁵ and 32.84×10⁵ Ns/m for ZE- and ZC-type soil beneath the 5-storey building, respectively. Table 5 shows that when the neighbouring building was at mid-height of the other building, the severity of the pounding increased; thus, the required damper capacity increased. Figure 8 presents

Table 5. Total damper capacities and supplemental damping ratios considering different soil types

Parameter		Vrsta tla														
		ZA			ZB			ZC			ZD			ZE		
		15/5	15/10	15/15	15/5	15/10	15/15	15/5	15/10	15/15	15/5	15/10	15/15	15/5	15/10	15/15
Case 1	ξ_d [%]	10	10	–	10	5	–	20	20	–	5	–	–	–	–	–
	Σcd ($\times 10^5$ Ns/m)	9.36	8.92	–	9.37	2.36	–	18.75	17.88	–	4.68	–	–	–	–	–
Case 2	ξ_d [%]	10	15	10	–	–	5	15	25	15	–	–	–	–	–	–
	Σcd ($\times 10^5$ Ns/m)	9.36	13.36	13.28	–	–	3.24	14.01	22.27	19.92	–	–	–	–	–	–
Case 3	ξ_d [%]	5	15	15	25	35	25	35	60	25	25	20	20	10	15	15
	Σcd ($\times 10^5$ Ns/m)	4.69	13.37	21.02	23.44	31.21	33.20	32.84	53.40	25.45	23.40	17.80	16.95	9.37	13.41	15.12

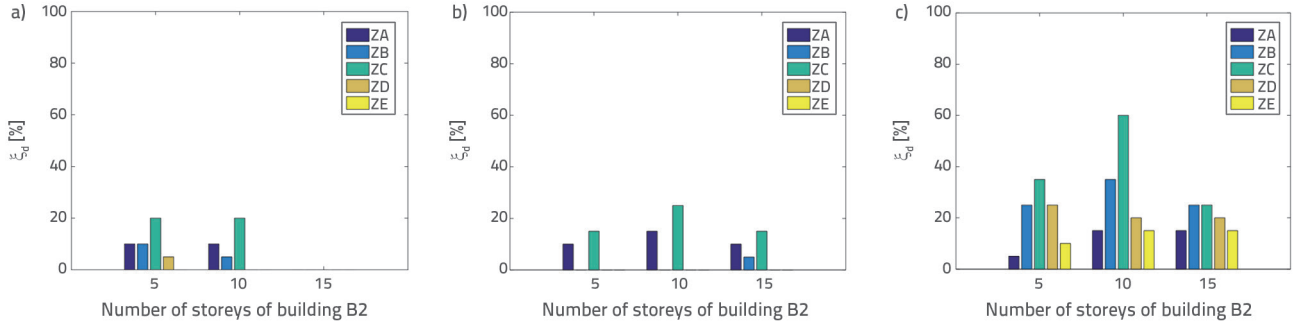

Figure 8. Supplemental damping ratios for different soil types under the Duzce earthquake: a) case 1; b) case 2; c) case 3

representative examples of the damping ratios obtained for building B2 with 5, 10, and 15 storeys exposed to the Duzce earthquake. No collisions were observed in the ZD- and ZE-type soils. Moreover, damping of up to 20 % for case 1 and 25 % for case 2 was required for the ZC-type soil. In addition, when a building was adjacent to a more flexible one (case 3), a higher damping ratio corresponding to a higher damper capacity was required (Figure 8.c). Note that for large damper capacities, nonlinear viscous dampers with velocity components lower than 1 should be used to avoid an excessive force that may damage the damper or have a detrimental unexpected effect on the seismic performance of buildings because of the possible high acceleration or force from dampers with large damping coefficients.

5. Conclusions

A comprehensive parametric study on adjacent structures with and without SSI was conducted to reveal the effect of soil type on the pounding-involved seismic behaviour. The CWT of impact forces was performed to compare and gain insight into the responses of fixed- and flexible-base adjacent structures with respect to the frequency contents of the signals. LVDs between adjacent floors were placed as a pounding protection measure. The required supplemental damping ratio of the LVDs was determined through optimisation analysis under different structural configurations and soil types to verify the effect of SSI on structural damping. The results of this study are summarised as follows.

1. The number and severity of pounding incidents highly depend on the rigidity of the neighbouring building and on whether the SSI effect is considered. Note that the impact forces of both flexible and fixed-base buildings are augmented when they are adjacent to a more flexible building. However, the impact forces increased by up to 36 and 44 times under the Duzce and Kobe earthquakes, respectively, when considering SSI in case 3.
2. Regarding building height, considering SSI, impacts occurred approximately 10 s earlier for lower structures, as indicated by the wavelet scalograms of the pounding forces. In addition, the wavelet scalograms showed that the number and severity of impacts increased and extended over a long period. Considering the SSI, the frequencies at which the impact forces were observed decreased by a maximum of 1/8 (as in the case of the Duzce earthquake for 5-storey building).

3. Collisions of buildings with SSI occur more often when the neighbouring building is stiffer, as compared with when the neighbouring building is more flexible. Therefore, the incorporation of SSI prevents numerous collisions in flexible structures. This is because of the significant contribution of foundation moments to the overall response in stiffer structural systems. Stiffer buildings with SSI are susceptible to collisions, similar to flexible buildings with fixed bases.
4. As the flexibility of the adjacent building increased, the required supplemental damping ratio of the LVDs increased to prevent pounding. However, for the 14-storey building in case 1, even if dampers were required for a fixed base, when considering the SSI, dampers were note required to be installed.
5. The number of collisions and severity of the impact forces decrease when the heights of the buildings are close to each other; therefore, the capacity of the LVDs is reduced. A decrease of up to 75 % in the damping ratios of the LVDs was obtained when SSI was considered, as in case 2 for the 13-storey building.
6. The frequency components at which the maximum impact force occurs vary according to the earthquake.
7. Softer soils are advantageous for avoiding collisions when the buildings are stiffer. For more flexible soil, such as ZE, the required damping coefficient becomes smaller, such as 9.37×10^5 Ns/m, and 32.84×10^5 Ns/m for ZC-type soil beneath the 5-storey building.
8. The greatest damping coefficients were obtained for the ZC-type soil. For the Duzce earthquake example, in cases 1 and 2, as for the ZD- and ZE-type soils, no collision was observed. Moreover, damping of up to 20 %, 25 %, and 60 % for cases 1, 2, and 3, respectively, was necessary for the ZC-type soil.
9. Considering soil during seismic analysis has significance for characterising the pounding behaviour under seismic excitations. The difference between the fixed-base and flexible-base structures in terms of the LVD capacity to prevent pounding has proven that as the height of the building increases, soil flexibility has an advantageous effect on the damper capacity.

REFERENCES

[1] Cole, G.L., Dhakal, R.P., Turner, F.M.: Building pounding damage observed in the 2011 Christchurch earthquake, Earthquake Engineering and Structural Dynamics, 41 (2012), pp. 893-913, https://doi.org/10.1002/eqe.1164

[2] Yazgan, U., Oyguç, R., Ergüven, M.E., Celep, Z.: Seismic performance of buildings during 2011 Van earthquakes and rebuilding efforts, Earthquake Engineering and Structural Dynamics, 15 (2016), pp. 591–606, https://doi.org/10.1007/s11803-016-0346-9

[3] Shrestha, B., Hao, H.: Building Pounding Damages Observed during the 2015 Gorkha Earthquake, Journal of Performance of Constructed Facilities, 32 (2018) 2, https://doi.org/10.1061/(asce)cf.1943-5509.0001134

[4] Kasai, K., Maison, B.F.: Building pounding damage during the 1989 Loma Prieta earthquake, Engineering Structures, 19 (1997), pp. 195–207, https://doi.org/10.1016/S0141-0296(96)00082-X

[5] Efraimiadou, S., Hatzigeorgiou, G.D., Beskos, D.E.: Structural pounding between adjacent buildings subjected to strong ground motions Part I: The effect of different structures arrangement, Earthquake Engineering and Structural Dynamics, 42 (2013), pp. 1509-1528, https://doi.org/10.1002/eqe.2285

[6] Moustafa, A., Mahmoud, S.: Damage assessment of adjacent buildings under earthquake loads, Engineering Structures, 61 (2014), pp. 153-165, https://doi.org/10.1016/j.engstruct.2014.01.004

[7] Sołtysik, B., Jankowski, R.: Non-linear strain rate analysis of earthquake-induced pounding between steel buildings. International Journal of Earth Sciences and Engineering, 6 (2013) 3, pp. 429-433.

[8] Mavronicola, E.A., Polycarpou, P.C., Komodromos, P.: Effect of ground motion directionality on the seismic response of base isolated buildings pounding against adjacent structures, Engineering Structures, 207 (2020), 110202, https://doi.org/10.1016/j.engstruct.2020.110202

[9] Mohebi, B., Yazdanpanah, O., Kazemi, F., Formisano, A.: Seismic damage diagnosis in adjacent steel and RC MRFs considering pounding effects through improved wavelet-based damage-sensitive feature, Journal of Building Engineering, 33 (2021), 101847, https://doi.org/10.1016/j.jobe.2020.101847

[10] Kazemi, F., Miari, M., Jankowski, R.: Investigating the effects of structural pounding on the seismic performance of adjacent RC and steel MRFs, Bulletin of Earthquake Engineering, 19 (2021) 1, pp. 317-343, https://doi.org/10.1007/s10518-020-00985-y

[11] Kazemi, F., Mohebi, B., Jankowski, R.: Predicting the seismic collapse capacity of adjacent SMRFs retrofitted with fluid viscous dampers in pounding condition, Mechanical Systems and Signal Processing, 161 (2021), 107939, https://doi.org/10.1016/j.ymssp.2021.107939

[12] Elwardany, H., Jankowski, R., Seleemah, A.: Mitigating the seismic pounding of multi-story buildings in series using linear and nonlinear fluid viscous dampers, Archives of Civil and Mechanical Engineering, 21 (2021) 4, Article number 137, https://doi.org/10.1007/s43452-021-00249-9

[13] Korzec, A., Jankowski, R.: Extended Newmark method to assess stability of slope under bidirectional seismic loading, Soil Dynamics and Earthquake Engineering, 143 (2021), 106600, https://doi.org/10.1016/j.soildyn.2021.106600

[14] Kamgar, R., Tavakoli, R., Rahgozar, P., Jankowski, R.: Application of discrete wavelet transform in seismic nonlinear analysis of soil-structure interaction problems, Earthquake Spectra, 37 (2021) 3, pp. 1980-2012, https://doi.org/10.1177/8755293020988027

[15] Minasidis, G., Hatzigeorgiou, G.D., Beskos, D.E.: SSI in steel frames subjected to near-fault earthquakes, Soil Dynamics and Earthquake Engineering, 66 (2014), pp. 56-68, https://doi.org/10.1016/j.soildyn.2014.06.030

[16] Far, H.: Advanced computation methods for soil-structure interaction analysis of structures resting on soft soils, International Journal of Geotechnical Engineering, 13 (2019) 4, pp. 352-359, https://doi.org/10.1080/19386362.2017.1354510

[17] Elwardany, H., Seleemah, A., Jankowski, R., El-Khoriby, S.: Influence of soil-structure interaction on seismic pounding between steel frame buildings considering the effect of infill panels, Bulletin of Earthquake Engineering, 17 (2019) 11, pp. 6165-6202, https://doi.org/10.1007/s10518-019-00713-1

[18] Sanghai, S.S., Pawade, P.Y.: Effectiveness of friction dampers on seismic response of structure considering soil-structure interaction, GRAĐEVINAR, 72 (2020) 1, pp. 33-44, https://doi.org/10.14256/JCE.1982.2017

[19] Dhehbiya, G., Salah, K.: Effects and dynamic behaviour of soil - framed structure interaction, GRAĐEVINAR, 74 (2022) 1, pp. 9-20, https://doi.org/10.14256/JCE.2301.2017

[20] Muhsin, A.A., Risan, H.K.: Influence of near-fault characteristics on inelastic response of multi-storey building with intensity measurement analysis, GRAĐEVINAR, 73 (2021) 11, pp. 1081-1092, https://doi.org/10.14256/JCE.2898.2020

[21] Mertol, H.C., Tunc, G., Akis, T.: Evaluation of masonry buildings and mosques after Sivrice earthquake, GRAĐEVINAR, 73 (2021) 9, pp. 881-892, https://doi.org/10.14256/JCE.3101.2021

[22] Miari, M., Choong, K.K., Jankowski, R.: Seismic pounding between adjacent buildings: Identification of parameters soil interaction issues and mitigation measures, Soil Dynamics and Earthquake Engineering, 121 (2019), pp. 135-150, https://doi.org/10.1016/j.soildyn.2019.02.024

[23] Mahmoud, S., Abd-Elhamed, A., Jankowski, R.: Earthquake-induced pounding between equal height multi-storey buildings considering soil-structure interaction, Bulletin of Earthquake Engineering, 11 (2013) 4, pp. 1021-1048, https://doi.org/10.1007/s10518-012-9411-6

[24] Ghandil, M., Aldaikh, H.: Damage-based seismic planar pounding analysis of adjacent symmetric buildings considering inelastic structure–soil–structure interaction, Earthquake Engineering and Structural Dynamics, 46 (2017), pp. 1141-1159, https://doi.org/10.1002/eqe.2848

[25] Madani, B., Behnamfar, F., Tajmir Riahi, H.: Dynamic response of structures subjected to pounding and structure–soil–structure interaction, Soil Dynamics and Earthquake Engineering, 78 (2015), pp. 46-60, https://doi.org/10.1016/j.soildyn.2015.07.002

[26] Naserkhaki, S., Abdul Aziz, F.N.A., Pourmohammad, H.: Earthquake induced pounding between adjacent buildings considering soil-structure interaction, Earthquake Engineering and Engineering Vibration, 11, (2012), pp. 343-358, https://doi.org/10.1007/s11803-012-0126-0

[27] Kermani, M., Saadatpour, M.M., Behnamfar, F., Ghandil, M.: Effects of seismic pounding between adjacent structures considering structure-soil-structure interaction, Scientia Iranica, 27 (2020), 5, pp. 2230-2246, https://doi.org/10.24200/sci.2019.5405.1255

[28] Miari, M., Jankowski, R.: Incremental dynamic analysis and fragility assessment of buildings founded on different soil types experiencing structural pounding during earthquakes, Engineering Structures, 252 (2022), 113118, https://doi.org/10.1016/j.engstruct.2021.113118

[29] Sarcheshmehpour, M., Estekanchi, H.E., Ghannad, M.A.: Optimum placement of supplementary viscous dampers for seismic rehabilitation of steel frames considering soil–structure interaction, Structural Design of Tall and Special Buildings, 29 (2020), e1682, https://doi.org/10.1002/tal.1682

[30] Kandemir-Mazanoglu, E.C., Mazanoglu, K.: An optimization study for viscous dampers between adjacent buildings, Mechanical Systems and Signal Processing, 89 (2017), pp. 88-96, https://doi.org/10.1016/j.ymssp.2016.06.001

[31] Ramirez, O.M., Constantinou, M.C., Kircher, C.A., Whittaker, A.S., Johnson, M.W., Gomez, J., Chrysostomou, C.Z.: Development and evaluation of simplified procedures for analysis and design of buildings with passive energy dissipation systems-Revision 01, New York: Multidisciplinary Center for Earthquake Engineering Research (MCEER), 2001.

[32] Whittaker, A.S., Constantinou, M.C., Ramirez, O.M., Johnson, M.W., Chrysostomou, C.Z.: Equivalent lateral force and modal analysis procedures of the 2000 NEHRP Provisions for buildings with damping systems, Earthquake Spectra, 19 (2003) 4, pp. 959-980, https://doi.org/10.1193/1.1622391

[33] Whittle, J.K., Williams, M.S., Karavasilis, T.L., Blakeborough, A.: A comparison of viscous damper placement methods for improving seismic building design, Journal of Earthquake Engineering, 16 (2012) 4, pp. 540-560, https://doi.org/10.1080/13632469.2011.653864

[34] Lin, W.H., Chopra, A.K.: Earthquake response of elastic SDF systems with non-linear fluid viscous dampers, Earthquake Engineering and Structural Dynamics, 31 (2002) 9, pp. 1623-1642, https://doi.org/10.1002/eqe.179

[35] Agrawal, A.K., Yang, J.N.: Design of passive energy dissipation systems based on LQR control methods, Journal of Intelligent Material Systems and Structures, 10 (1999) 12, pp. 933-944, https://doi.org/10.1106/FB58-N1DG-ECJT-B8H4

[36] The Mathworks Inc., MATLAB: The language of technical computing, 9.1.0.441655 (R2016b), Natick, MA, USA.

[37] Anagnostopoulos, S.A.: Pounding of buildings in series during earthquakes, Earthquake Engineering and Structural Dynamics, 16 (1988) 3, pp. 443-456, https://doi.org/10.1002/eqe.4290160311

[38] Davis, R.: Pounding of buildings modelled by an impact oscillator, Earthquake Engineering and Structural Dynamics, 21 (1992), pp. 253-274, https://doi.org/10.1002/eqe.4290210305

[39] Jankowski R.: Non-linear viscoelastic modelling of earthquake-induced structural pounding, Earthquake Engineering and Structural Dynamics, 34 (2005) 6, pp. 595-611, https://doi.org/10.1002/eqe.434

[40] Pantelides, C.P., Ma, X.: Linear and nonlinear pounding of structural systems, Computers and Structures, 6 (1998) 1, pp. 79-92, https://doi.org/10.1016/S0045-7949(97)00045-X

[41] Karayannis, C.G., Favvata, M.J.: Earthquake-induced interaction between adjacent reinforced concrete structures with non-equal heights, Earthquake Engineering and Structural Dynamics, 34 (2005) 1, pp. 1-20, https://doi.org/10.1002/eqe.398

[42] Mahmoud, S., Jankowski, R.: Elastic and inelastic multi-storey buildings under earthquake excitation with the effect of pounding, Journal of Applied Sciences, 9 (2009) 18, pp. 3250-3262, https://doi.org/10.3923/jas.2009.3250.3262

[43] Khatiwada, S., Chouw, N., Butterworth, J.W.: A generic structural pounding model using numerically exact displacement proportional damping, Engineering Structures, 62-63 (2014), pp. 33-41, https://doi.org/10.1016/j.engstruct.2014.01.016

[44] Azevedo, J., Bento, R.: Design criteria for buildings subjected to pounding, Proceedings 11th World Conference on Earthquake Engineering 1996, Paper no. 1063, Acapulco, Mexico.

[45] Wolf, J.P.: Spring-dashpot-mass models for foundation vibrations, Earthquake Engineering and Structural Dynamics, 26 (1997) 9, pp. 931-949, https://doi.org/10.1002/(SICI)1096-9845(199709)26:9<931::AID-EQE686>3.0.CO;2-M

[46] Republic of Turkey Ministry of Interior Disaster and Emergency Management Authority, Turkey Building Earthquake Code TBEC 2018, Ankara, Turkey.

[47] American Society of Civil Engineers, Minimum design loads and associated criteria for buildings and other structures: ASCE/SEI 7-16, 2017, United States.

[48] Gercek, H.: Poisson"s ratio values for rocks, International Journal of Rock Mechanics and Mining Sciences, 44 (2007) 1, pp. 1-13, https://doi.org/10.1016/j.ijrmms.2006.04.011

[49] IBC. International Building Code, International Code Council 2012.

[50] Deere, D.U., Miller, R.P.: Engineering classification and index properties for intact rock, University of Illinois, Illinois, 1966.

[51] Veletsos, A.S., Ventura, C.E.: Modal analysis of non-classically damped linear systems, Earthquake Engineering and Structural Dynamics, 14 (1986), pp. 217–243, https://doi.org/10.1002/eqe.4290140205

[52] PEER Ground Motion Database. https://ngawest2.berkeley.edu/, 10.02.2021.

[53] AFAD Turkish Accelerometric Database and Analysis System. https://tadas.afad.gov.tr/list-event., 10.02.2021.

[54] Xing, S., Halling, M.W., Meng, Q.: Structural Pounding Detection by Using Wavelet Scalogram, Advances in Acoustics and Vibration, (2012), Article ID 805141, https://doi.org/10.1155/2012/805141

[55] Li, H., Yi, T., Gu, M., Huo, L.: Evaluation of earthquake-induced structural damages by wavelet transform, Progress in Natural Science, 19 (2009) 4, pp. 461-470, https://doi.org/10.1016/j.pnsc.2008.09.002

[56] Misiti, M., Misiti, Y., Oppenheim, G., Poggi, J.M.: Wavelet Toolbox: The MathWorks, 2014.

[57] Chun, L.C., Zhengding, Q.: A method based on Morlet wavelet for extracting vibration signal envelope. 5th International Conference on Signal Processing Proceedings. 16th World Computer Congress, 1 (2000), pp. 337-340.

[58] Sheen, Y.T., Hung, C.K.: Constructing a wavelet-based envelope function for vibration signal analysis, Mechanical Systems and Signal Processing, 18 (2004), pp. 119-126, https://doi.org/10.1016/S0888-3270(03)00046-3

[59] Heidari, A., Majidi, N.: Earthquake acceleration analysis using wavelet method, Earthquake Engineering and Engineering Vibration, 20 (2021) 1, pp. 113-126, https://doi.org/10.1007/s11803-021-2009-8

[60] Lin, J., Qu, L.: Feature extraction based on Morlet wavelet and its application for mechanical fault diagnosis, Journal of Sound and Vibration, 234 (2004), pp. 135-148, https://doi.org/10.1006/jsvi.2000.2864